Effect of Pressure on the Freezing of Pure Fluids and Mixtures Confined in Nanopores†

Benoit Coasne,[#] J. Czwartos,[§] M. Sliwinska-Bartkowiak,[§] and Keith E. Gubbins*,[‡]

Institut Charles Gerhardt Montpellier, CNRS (UMR5253), Université Montpellier 2, ENSCM, Place Eugène Bataillon, 34095 Montpellier Cedex 05, France, Institute of Physics, Adam Mickiewicz University, Umultowska 85, 61-614 Poznan, Poland, Center for High Performance Simulation and Department of Chemical and Biomolecular Engineering, North Carolina State University, Raleigh, North Carolina 27695-7905

Received: April 6, 2009; Revised Manuscript Received: June 25, 2009

Monte Carlo simulations combined with the parallel tempering technique are used to study the freezing of Ar, CH_4, and their mixtures in a slit graphite nanopore. For all systems, the solid/liquid coexistence line is located at higher temperature than that for the bulk phase, as expected for fluids for which the wall/fluid interaction is stronger than the fluid/fluid interaction. In the case of the mixtures, the phase diagram for the confined system is of the same type as that for the bulk (azeotropic). It is also found that the freezing temperatures for the confined fluids and mixture are much more affected by pressure than those for the bulk phase. By calculating the isothermal compressibility of the confined fluids and determining the slope of the solid/liquid coexistence line (T,P) from the Clapeyron equation, we show that such a strong effect of pressure is not related to reduced compressibility within the pores. On the other hand, the pressure dependence of the in-pore freezing temperature is correctly described in the frame of the model proposed by Miyahara et al. [Miyahara, M.; Kanda, H.; Shibao, M.; Higashitani, K. *J. Chem. Phys.* **2000**, *112*, 9909.], which is based on the pressure difference between the bulk and confined phases (capillary effect). In this model, a change in the in-pore freezing temperature with pressure is explained by a drastic change in the in-pore pressure, which varies very sharply with the bulk external pressure. We present an extended version of this model to confined systems for which an increase in the freezing temperature is observed.

I. Introduction

Freezing and melting of fluids or mixtures confined at the nanoscale is relevant to practical applications involving lubrication, adhesion, nanotribology, and fabrication of nanomaterials.[1,2] For instance, the use of nanoporous solids as templates to obtain nanomaterials such as composites, nanowires, or nanotubes is receiving increasing attention.[3−9] Freezing in porous media has also been widely employed in the characterization of porous materials using the method of thermoporometry.[10] In this method, the change in the freezing temperature is related to the pore size through the Gibbs−Thomson equation. From a fundamental point of view, the freezing of systems confined in nanopores can be used to estimate the effect of confinement, surface forces, and reduced dimensionality on the thermodynamics and dynamics of fluids. Upon reducing the width of the confined space to approach the range of the intermolecular forces, significant shifts in the freezing temperature are observed, and in some cases, new surface- or confinement-induced phases occur.[2,11,12] Previous experimental, molecular simulation, and theoretical studies have shown that, for simple fluids and pore geometries, the freezing temperature can be described as a function of the reduced pore size $H^* = H/\sigma$ (H is the pore width, and σ the diameter of an adsorbate molecule) and the ratio of the wall/fluid (wf) to the fluid/fluid (ff) interactions, $\alpha \sim C\rho_w\varepsilon_{wf}/\varepsilon_{ff}$, where ρ_w and ε are the density of wall atoms and the potential well depth, respectively, and C is a constant that depends on the wall geometry. The freezing temperature T_f is decreased compared to the bulk value, T_f^0, for $\alpha < \sim 1$, while it is increased for $\alpha > \sim 1$. The magnitude of the shift in the transition temperature depends on H, while the appearance of surface- or confinement-induced phases usually depends on a combination of effects from H and α (for a recent review on the effects of confinement and surface forces on freezing, see ref 2).

For sufficiently large pores, the shift in the freezing temperature $\Delta T_f \equiv T_f - T_f^0$ can be related to the pore width H^* using the Gibbs−Thomson equation, which is obtained either by equating the free energies of the confined liquid and solid phases[13] or by determining the temperature at which the chemical potential of the confined solid equals that of the bulk reservoir.[14] In agreement with the Gibbs−Thomson equation, early experiments performed for pores larger than 6−7 nm showed a linear relation between the in-pore freezing temperature and the inverse pore width. However, the equation fails to predict the freezing temperature for smaller pores. Differential scanning calorimetry and dielectric relaxation spectrometry for CCl_4 confined in controlled porous glasses showed that the Gibbs−Thomson equation fails to describe the shift in the freezing temperature for pores smaller than $\sim 15\sigma$ (i.e., $\sim$7.5 nm).[15] Similarly, the equation fails for CCl_4 in activated carbon fibers (pore width of 1.1−1.7 nm).[16] This breakdown is due to the use of macroscopic concepts in the derivation of the Gibbs−Thomson equation, such as surface tension (implying an interface separating two bulk-like phases), and the failure to account for the strong inhomogeneity of the confined phase. Even when the Gibbs−Thomson equation is expected to apply, its use is usually limited by the unavailability of the surface tensions involved.

A qualitative understanding of the effects of confinement on freezing temperature can be obtained from the following

† Part of the "H. Ted Davis Special Section".
* To whom correspondence should be addressed. E-mail: keg@ncsu.edu.
[#] Université Montpellier 2.
[§] Adam Mickiewicz University.
[‡] North Carolina State University.

10.1021/jp9031699 CCC: $40.75
Published on Web 07/23/2009

reasoning, which does not rest on macroscopic arguments concerning surface tension. If we assume that the fluid molecules can be treated as Lennard-Jones particles, the bulk fluid will freeze at a temperature that is proportional to the parameter ε_{ff}. Similarly, we can expect that the freezing temperature for the confined phase will be proportional to ε_{eff}, which is an effective energy parameter that accounts for both the fluid/fluid and fluid/wall interactions in some average way. For strongly attractive walls, an increase in the freezing temperature with respect to the bulk is expected as ε_{eff} is larger than ε_{ff}. In contrast, a decrease in the freezing temperature is expected for weakly attractive pores as ε_{eff} is smaller than ε_{ff}. When $\varepsilon_{eff} \sim \varepsilon_{ff}$, the in-pore freezing temperature should be similar to that of the bulk. These predictions are supported by previous molecular simulations and experiments on the freezing and melting of simple fluids confined in various nanoporous materials (carbon pores, silica pores, mica plates in surface force apparatus, etc.).[11,12,15−22] Since carbon and mica surfaces are strongly attractive, we expect that a rise in freezing temperature is likely for many adsorbates that do not have strongly attractive (e.g., H-bonding) fluid/fluid interactions. Such systems exhibit large α values, that is, the ratio of the wall/fluid to the fluid/fluid interactions is larger than 1. On the other hand, we would not expect such an increase in T_f for water in these materials since α is smaller than 1.[11,12] Recent SFA experiments have confirmed this prediction by showing that water[23,24] and some alcohols (octanol, undecanol[25]) remain fluid-like, even for confined film thicknesses below 1 nm.

In contrast to the pore size H and the wall/fluid interaction, the effect of pressure on the freezing of confined systems has received considerably less attention.[26−30] In this paper, we report molecular simulations for Ar, CH_4, and their mixtures confined at three different pressures in a carbon nanopore having a width of 0.69 nm, which corresponds to $\sim 2\sigma$. The choice of such a small pore, which accommodates one layer of adsorbate, is motivated by the fact that we expect the largest effect of pressure for this system compared to the bulk. In these simulations, Ar and CH_4 are described as Lennard-Jones fluids. Following previous works, we study freezing in nanopores using bond order parameters and both positional and bond orientational pair correlation functions. The effect of pressure on the in-pore solid/liquid phase transition is discussed in light of calculations of (1) the isothermal compressibility of the confined fluid and (2) the slope of the solid/liquid coexistence line from the Clausius−Clapeyron equation. We also discuss the ability of the model proposed by Miyahara et al.[26] to predict the change in the freezing temperature of the confined fluid with pressure. Finally, we compare the solid/liquid phase diagram of the confined Ar/CH_4 mixture with its bulk counterpart and report its evolution with increasing pressure.

II. Computational Details

Freezing of Ar, CH_4, and their mixtures in a slit graphite nanopore with $H = 0.69$ nm $\approx 2\sigma$ ($\sigma = 0.3405$ nm for argon) was determined using the grand canonical Monte Carlo technique (GCMC).[31] This stochastic method simulates a system having a constant volume V (the pore with the adsorbed phase), in equilibrium with an infinite fictitious reservoir of particles imposing its chemical potential for each species, μ_{Ar} and μ_{CH4}, and its temperature, T. In order to circumvent the difficulty of particle deletion and insertion in dense phases such as liquids and solids, we combined the GCMC simulations with the parallel tempering technique. Full details of the GCMC and parallel tempering techniques used in this work have been described elsewhere.[32−34] The square section of the graphite slit pores was 7.62 nm × 7.62 nm ($\sim 22\sigma_{Ar} \times 22\sigma_{Ar}$). Periodic boundary conditions were applied in the directions (x, y) parallel to the pore walls. The fluid/fluid interactions Ar/Ar and CH_4/CH_4 were calculated using Lennard-Jones potentials with $\sigma_{Ar} = 0.3405$ nm, $\varepsilon_{Ar}/k_B = 119.8$ K, $\sigma_{CH4} = 0.381$ nm, and $\varepsilon_{CH4}/k_B = 148.1$ K. The cross-species parameters $\sigma_{Ar/CH4}$ and $\varepsilon_{Ar/CH4}$ were determined using the Lorentz−Berthelot rules. The slit graphite nanopore was described as an assembly of two structureless parallel walls. The interaction between the fluids and each pore wall was calculated using the Steele 10−4−3 potential[35]

$$U_{wf}(z) = 2\pi\rho_w\varepsilon_{wf}\sigma_{wf}^2\Delta\left[\frac{2}{5}\left(\frac{\sigma_{wf}}{z}\right)^{10} - \left(\frac{\sigma_{wf}}{z}\right)^4 - \left(\frac{\sigma_{wf}^4}{3\Delta(z + 0.61\Delta)^3}\right)\right] \quad (1)$$

where z is the distance between the adsorbed molecule and the graphite surface, Δ is the separation between graphite layers, 0.335 nm, and ρ_w is the atomic density of graphite layers, 114 nm^{-3}. The wall/fluid Lennard-Jones parameters $\varepsilon_{w/Ar}$, $\sigma_{w/Ar}$, $\varepsilon_{w/CH4}$, and $\sigma_{w/CH4}$ were determined by combining the wall/wall and fluid/fluid parameters using the Lorentz−Berthelot rules with the values $\varepsilon_{ww}/k_B = 28$ K and $\sigma_{ww} = 0.34$ nm for the carbon wall. Radhakrishnan et al.[11] have shown that the parameter $\alpha = \rho_w\varepsilon_{wf}\sigma_{wf}^2\Delta/\varepsilon_{ff}$, that is, the ratio of the wall/fluid to the fluid/fluid attractive interactions, can be used to describe the change in freezing temperature of a confined system. An increase (decrease) in the freezing temperature compared to the bulk is expected for $\alpha > \sim 1$ ($\alpha < \sim 1$). The α parameters for Ar and CH_4 confined in graphite pores are 2.14 and 2.16, respectively. The input parameters required in the GCMC simulations, $\mu_{Ar}(T,P)$ and $\mu_{CH4}(T,P)$ at a given pressure P and temperature T, were determined using the equation of state for Lennard-Jones mixtures of Johnson et al.[36] The number of particles in our simulations varies from 400−1200, depending on the mole fraction of the confined mixture and the pore width H. The number of replicas used in the parallel tempering is 16, and the temperature difference between two successive replicas is $\Delta T = 2$ or 3 K. We started with a well-equilibrated liquid configuration of the confined mixture and performed at least 10^5 Monte Carlo steps per particle to equilibrate the system using the parallel tempering technique. After equilibration of the system, density profiles, bond order parameters, and pair correlation functions were averaged in the course of a second simulation run.

Strong layering was observed due to the interaction with the attractive pore walls. Following previous works on the freezing of pure fluids in nanopores,[11,12,37−39] the structure of the confined system was investigated by calculating for each layer j of adsorbate the 2D bond order parameters $\Phi_{6,j}$. We determined $\Phi_{6,j}$ as the average value of the local order parameter $\Psi_{6,j}(\mathbf{r})$, which measures the hexagonal bond order at a position $\mathbf{r}$ of a particle located in the layer j[40,41]

$$\Psi_{6,j}(\mathbf{r}) = \frac{1}{N_b}\sum_{k=1}^{N_b}\exp(i6\theta_k) \qquad \text{with} \quad \Phi_{n,j} = \frac{\left|\int \Psi_{n,j}(\mathbf{r})d\mathbf{r}\right|}{\int d\mathbf{r}} \quad (2)$$

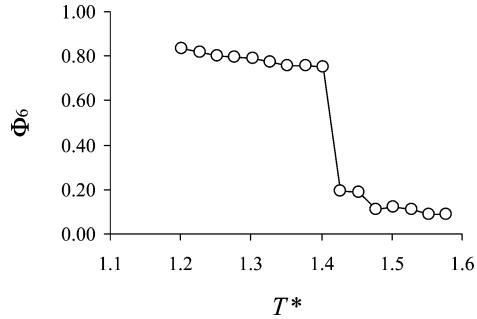

Figure 1. Average value of the 2D bond order parameter Φ_6 as a function of the temperature T^* for CH_4 confined at $P^* = 0.002$ in a slit graphite nanopore with $H^* = 2$. Temperatures and pressures are in reduced units with respect to σ_{Ar} and ε_{Ar}.

where $\theta_k$are the bond angles between the particle and each of its N_b nearest neighbors. $\Phi_{6,j}$ is close to 1 for a crystal layer having a triangular structure and close to 0 for a liquid layer. We also monitored the 2D in-plane positional and bond orientational pair correlation functions, $g_j(r)$ and $G_{6,j}(r)$.[32−34,39] The latter measures for each layer j the correlations between the local bond order parameter $\Psi_{6,j}(\mathbf{r})$ at two positions separated by a distance r

$$G_6(r) = \langle \Psi^*_{6,j}(0)\Psi_{6,j}(r)\rangle \quad (3)$$

III. Results and Discussion

A. Determination of the Freezing Temperature. All of the quantities (temperature, pore size, pressure, chemical potential, density, etc.) in the remainder of this paper are in reduced units with respect to the Lennard-Jones parameters for argon (σ_{Ar}, ε_{Ar}). We first report GCMC simulations for pure Ar and CH_4 confined in the graphite nanopore with $H^* = 2$ at three different pressures, $P^* = 0.002$, 0.011, and 0.064 (which correspond to 1, 5, and 25 atm, respectively). Here, we present, as an example, a detailed analysis of the results obtained for methane confined in the nanopore at $P^* = 0.002$. The results obtained for the two fluids and for the three pressures will be discussed in the next paragraph. Density profiles for confined argon and methane show that the pore $H^* = 2$ accommodates one adsorbed layer. The average value of the 2D bond order parameter for this confined layer, Φ_6, is shown in Figure 1 as a function of the temperature T^*. Upon freezing, Φ_6 sharply increases at $T^* \sim 1.4$, which reveals that the adsorbed film undergoes a liquid to crystal phase transition. Φ_6 varies from ~0.1 in the liquid region up to ~0.80 in the crystal region. This latter value suggests that the layers have a hexagonal crystal structure (triangular symmetry) with, however, some defects.

In-plane 2D positional $g(r)$ and orientational $G_6(r)$ pair correlation functions for CH_4 confined at $P^* = 0.002$ in the nanopore with $H^* = 2$ are presented for two temperatures in Figures 2 and 3, respectively. Correlations within each layer were determined up to a distance of half of the size of the simulation box. At $T^* = 1.58$, the confined layers exhibit a liquid-like behavior as revealed by the $g(r)$ function, which is characteristic of a phase having short-range positional order. This result is confirmed by the exponential decay observed in the $G_6(r)$ function; such a decay is typical of 2D liquid phases, which have short-range orientational order. On the other hand, at $T^* = 1.20$, the confined layers appear as 2D hexagonal crystals with long-range positional order, as can be seen from the features of the $g(r)$ function for this temperature; (i) the amplitude between the first and the second peak is close to 0, (ii) the second peak is split into two secondary peaks, and (iii) the third peak presents a shoulder on its right side. Moreover, the $G_6(r)$ function at this temperature has a constant average value, as expected for a hexagonal crystal layer with long-range orientational order. Analysis of the in-plane 2D pair correlation functions $g(r)$ and $G_6(r)$ corroborate the results shown in Figure 1 for the 2D bond order parameter Φ_6; the transition temperature between the crystal and liquid phases was found to be $T^* = 1.42$. For all molar compositions studied in this work, it seems that freezing of the confined layers involves a direct phase transition between a 2D crystal and a 2D liquid.

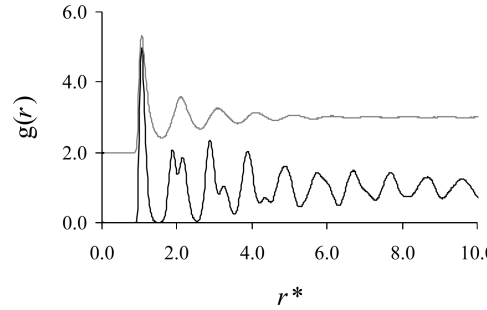

Figure 2. In-plane 2D positional pair correlation function $g(r)$ for CH_4 confined at $P^* = 0.002$ in a slit graphite nanopore with $H^* = 2$ at (black line) $T^* = 1.20$ and (gray line) $T^* = 1.58$. The $g(r)$ function for $T^* = 1.58$ has been shifted by +2.0 for the sake of clarity. Temperatures, pressures, and distances are in reduced units with respect to σ_{Ar} and ε_{Ar}.

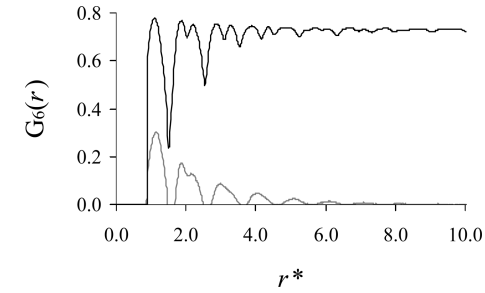

Figure 3. In-plane 2D orientational pair correlation function $G_6(r)$ for CH_4 confined at $P^* = 0.002$ in a slit graphite nanopore with $H^* = 2$ at (black line) $T^* = 1.20$ and (gray line) $T^* = 1.58$. Temperatures, pressures, and distances are in reduced units with respect to σ_{Ar} and ε_{Ar}.

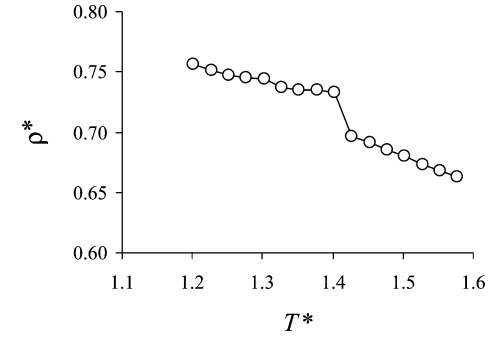

Figure 4. Density of CH_4 confined at $P^* = 0.002$ in a slit graphite nanopore with $H^* = 2$ as a function of the temperature T^*.

The density of CH_4 confined at $P^* = 0.002$ in the nanopore with $H^* = 2$ is shown in Figure 4 as a function of T^*. The pore volume used in these density calculations was estimated using the pore size diminished by $\sigma_{w/CH4}$ in order to account for the excluded volume due to the short-range repulsion with the pore walls. Upon freezing, ρ^* increases at $T^*_f = 1.42$ from

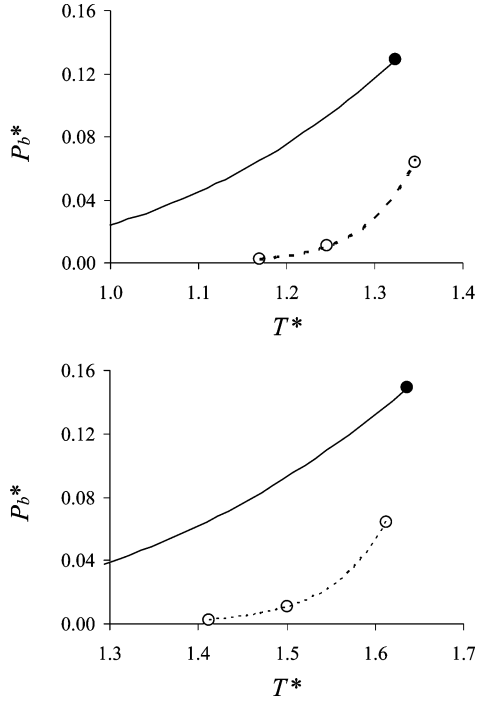

Figure 5. (open circles) Effect of bulk-phase pressure on solid/liquid coexistence (T^*,P^*) for argon (top) and methane (bottom) confined in a slit graphite nanopore with $H^* = 2$. The dashed lines are exponential fits of the simulated data. The black solid line indicates the bulk gas/liquid coexistence line, which ends at the critical point marked by the closed circle (data taken from the work of Kofke[43]). Note that the bulk gas/liquid coexistence line differs between the two fluids as the data are reduced in each case with respect to σ_{Ar} and ε_{Ar}.

$\rho_L^* = 0.70$ in the liquid phase up to $\rho_S^* = 0.73$ in the crystal phase. The freezing temperature for the confined mixture, $T_f^* = 1.42$, is much larger than the bulk freezing point, $T_f^{*,bulk} \sim 0.85$, and corresponds to a relative increase of ~1.7. The same analysis for pure argon confined at $P^* = 0.002$ in the nanopore with $H^* = 2$ also reveals that the in-pore freezing temperature is larger than that for the bulk (the relative increase in the freezing temperature is also 1.7 for this fluid). The larger freezing temperatures for confined argon and methane compared with those for the bulk can be explained by the fact that the wall/fluid interactions are stronger than the fluid/fluid interactions for both Ar and CH_4, $\alpha_{Ar} = 2.14$ and $\alpha_{CH4} = 2.16$.[2,12] Finally, the sharp increase observed in the 2D bond order parameter Φ_6 and the CH_4 mole fraction suggest that the freezing of the confined system is a first-order transition, as has been found in previous works on fluids in nanopores.[12,37] Thanks to the use of the parallel tempering technique, in which both the liquid and crystal phases are simulated in the same run, we expect the results presented to correspond to the thermodynamic equilibrium state. In our previous work,[32] it has been shown that simulations of the melting and freezing phenomena give similar results, provided that the parallel tempering method is used and a significant fraction of the swap trial moves are accepted.[42] Moreover, Hung et al.[37] showed for pure fluids that this technique gives the same results as those obtained from free-energy calculations.

B. Effect of Pressure on Freezing. Figure 5 shows the solid/liquid coexistence line (T^*,P^*) for argon and methane confined at three different bulk-phase pressures in the slit nanopore with $H^* = 2$. We also report the bulk gas/liquid coexistence line[43] to help to locate the in-pore phase diagrams with respect to the bulk. Due to the positive shift in the freezing temperature, the in-pore solid/liquid coexistence line is located in a region corresponding to the gas phase for the bulk. The increase in the freezing temperature for the confined system depends strongly on the pressure; for instance, $T_f^* = 1.17$ at $P^* = 0.002$ and $T_f^* = 1.35$ at $P^* = 0.06$ for argon. Such a shift, $\Delta T_f^* \sim 0.2$, is 10 times larger than that for bulk argon $\Delta T_f^* < 0.02$ for the same change in pressure (see Figure 1 in ref 44). Similarly, the freezing temperature for confined methane drastically increases with pressure compared to the bulk solid/liquid coexistence. This result is in agreement with previous works in which it was shown that the solid/liquid coexistence for a confined system is much more affected by the pressure than the bulk.[26−28]

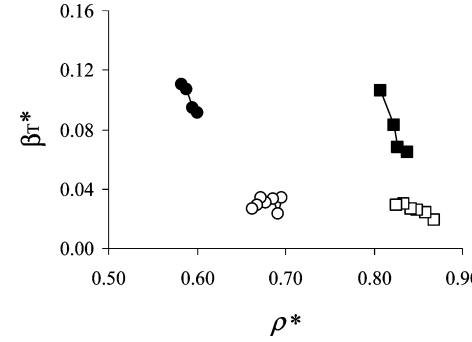

Figure 6. Isothermal compressibility β_T^* as a function of density ρ^* for argon (squares) and methane (circles). The closed and open symbols are for the bulk fluid and the fluid confined in the slit graphite nanopore with $H^* = 2$, respectively. The uncertainty in the calculated isothermal compressibility is ±0.02. Data are in reduced units with respect to σ_{Ar} and ε_{Ar}.

For a bulk system, the dependence of the freezing temperature on pressure is usually weak and is due to the low isothermal compressibility of most liquids. In order to clarify the role of pressure on the freezing of confined fluids, we determined the reduced isothermal compressibility $\beta_T^* = (\beta_T \varepsilon_{Ar}/\sigma_{Ar}^3)$, where $\beta_T = -(1/V)(\partial V/\partial P)_T$, for liquid argon and methane confined in the slit graphite nanopore with $H^* = 2$. The latter was determined from the fluctuations over the number of atoms δN in the GCMC runs using the following equation[45]

$$\beta_T^* = \frac{V^* \langle \delta N^2 \rangle}{N^2 T^*} \tag{4}$$

where N, T^*, and V^* are the number of atoms, the reduced temperature, and the reduced volume, respectively. The isothermal compressibility β_T^* for argon and methane in the nanopore with $H^* = 2$ is shown in Figure 6 as a function of the density ρ^*. We also report the data for bulk argon and methane in the liquid phase. For both fluids, the isothermal compressibility for the confined system is smaller than that for the bulk phase; β_T^* for confined argon and methane is about 50 and 33% of the bulk value, respectively. Such a result can be explained by the poor fluctuations in the number of particles for the in-pore fluid, which are limited due to the strong confinement in the slit pore geometry (atoms can be inserted or deleted only along two dimensions instead of three dimensions for a bulk system). The lower compressibility for the confined fluids suggests that the significant pressure dependence of the in-pore freezing temperature (Figure 5) cannot be related to the compressibility of the confined fluid. On the contrary, the low isothermal compressibility for the confined fluids suggest that the in-pore freezing temperature may depend weakly on pressure.

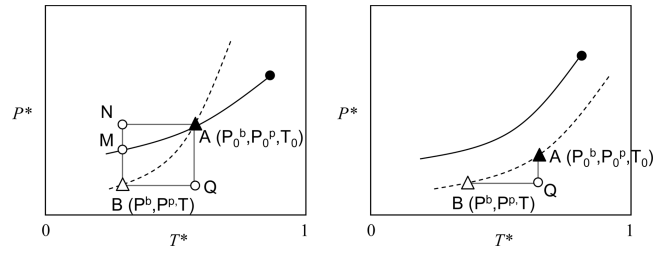

Figure 7. Two possibilities for the in-pore liquid/solid phase diagrams in the (P,T) plane (schematic). The in-pore solid/liquid coexistence curve is represented as the dashed line. The solid line corresponds to the bulk gas/liquid coexistence curve, which ends at the critical point marked by the closed circle. A path AB along the in-pore solid/liquid coexistence line is shown for model consideration. In the first situation (left), the path passing through $B(P^b,P^p,T)$ crosses the bulk gas/liquid coexistence curve at $A(P_0^b,P_0^p,T_0)$ (the superscripts p and b denote the in-pore and bulk pressures, respectively). AB for the bulk system can be decomposed as an isobaric path AN in the bulk liquid phase and the sum of an isothermal path NM in the bulk liquid phase and an isothermal path MB in the bulk gas phase. In the second situation (right), the path passing through $A(P_0^b,P_0^p,T_0)$ and $B(P^b,P^p,T)$ does not cross the bulk gas/liquid coexistence curve. In this case, AB for the bulk system can be decomposed as an isothermal path AQ and an isobaric path QB, both in the bulk gas phase. For both situations, AB for the confined system can be decomposed as the sum of an isothermal path AQ and an isobaric path QB in the confined liquid phase.

Miyahara et al. proposed a simple thermodynamic model to explain the large effect of pressure on freezing of confined fluids.[26] In what follows, the superscripts p and b denote the in-pore and bulk phases, while the subscripts G, L, and S indicate the gas, liquid, and solid phases. Suppose that the in-pore solid/liquid coexistence (T,P) curve passes through a point B, as shown in Figure 7. The bulk fluid is at a pressure P^b, while the fluid confined in the pore is at an effective pressure P^p due to the interaction with the pore wall and the capillary effect (surface tension effect leading to a pressure difference between the in-pore and bulk phases). Considering the in-pore solid/liquid coexistence, there are two possible situations that are depicted in Figure 7. The first corresponds to the case when the in-pore solid/liquid coexistence line crosses the bulk gas/liquid saturation curve. In this case, the path passing through B (P^b,P^p,T) crosses the bulk gas/liquid coexistence curve at A (P_0^b,P_0^p,T_0). The second situation, which has not been addressed by Miyahara and co-workers, corresponds to the case where the in-pore solid/liquid coexistence line does not cross the gas/liquid saturation curve but remains in the bulk vapor phase up to temperatures above the bulk critical temperature. As can be seen in Figure 5, both argon and methane in the slit graphite nanopore with $H^* = 2$ fall into the second category. On the other hand, other simulation results by Miyahara and co-workers[26−28] suggest that for larger pores, most systems belong to the first category.

We now derive a more general version of the model of Miyahara et al.,[26] extending it to any confined system for which an increase in freezing temperature occurs and showing that it remains valid even without some assumptions made in its original version. In what follows, we do not use superscripts p and b for the temperatures as we assume that the confined and bulk phases are at the same temperature (thermal equilibrium). We address the two situations shown in Figure 7. We first consider the case where the in-pore solid/liquid coexistence line crosses the bulk gas/liquid saturation curve (left figure in Figure 7). An infinitesimal change in the chemical potential along one of these paths can be expressed as

$$d\mu = -S dT + V dP \tag{5}$$

By integrating eq 5 for the bulk system along the isobaric path from $A(P_0^b,P_0^p,T_0)$ to $N(P_0^b,P_N^p,T)$ and the isothermal path from $N(P_0^b,P_N^p,T)$ to $B(P^b,P^p,T)$, one obtains

$$\begin{aligned} \Delta\mu_{AN}^b &= -\int_{T_0}^{T} S dT \\ \Delta\mu_{NB}^b &= \int_{P_N^b}^{P^b} V dP^b \end{aligned} \tag{6}$$

Given that AN is located in the bulk liquid region and assuming that the entropy of the bulk liquid, S_L^b, is independent of the temperature over this range, integration of the first equation in eq 6 leads to

$$\Delta\mu_{AN}^b = -S_L^b(T - T_0) \tag{7}$$

The second equation in eq 6 can be decomposed as an integral in the bulk liquid region between N and M and an integral in the bulk gas region from M to B

$$\Delta\mu_{NB}^b = \int_{P_N^b}^{P_M^b} V_L^b dP^b + \int_{P_M^b}^{P^b} V_G^b dP^b \tag{8}$$

where V_L^b and V_G^b are the molar volumes of the bulk liquid and gas phases, respectively. Given that $V_L^b \ll V_G^b$, the first integral can be neglected, and assuming the bulk vapor phase can be treated as an ideal gas, integration of eq 8 leads to

$$\Delta\mu_{NB}^b = RT \ln\left(\frac{P^b}{P_M^b}\right) \tag{9}$$

By adding eqs 7 and 9, one obtains the change in chemical potential for the bulk system along the path AB

$$\Delta\mu_{AB}^b = -S_L^b(T - T_0) + RT \ln\left(\frac{P^b}{P_M^b}\right) \tag{10}$$

If the in-pore solid/liquid coexistence line does not cross the bulk gas/liquid saturation curve (second situation in Figure 7), AB for the bulk system can simply be decomposed as an isothermal path and an isobaric path in the bulk gas phase. By integrating eq 5 for the bulk system along the isothermal path from $A(P_0^b,P_0^p,T_0)$ to $Q(P^b,P_Q^p,T_0)$ and the isobaric path from $Q(P^b,P_Q^p,T_0)$ to $B(P^b,P^p,T)$, one obtains

$$\begin{aligned} \Delta\mu_{AQ}^b &= \int_{P_0^b}^{P^b} V dP^b \\ \Delta\mu_{QB}^b &= -\int_{T_0}^{T} S dT \end{aligned} \tag{11}$$

Given that AQ is located in the bulk gas region and assuming that the bulk vapor phase can be treated as an ideal gas, integration of eq 11 leads to

$$\Delta\mu_{AQ}^b = RT_0 \ln\left(\frac{P^b}{P_0^b}\right) \tag{12}$$

QB is located in the bulk gas region, and assuming that the entropy of the bulk gas, S_G^b, is independent of the temperature in this temperature range (which implies that AB corresponds to a small change along the in-pore coexistence line), integration of the second equation in eq 11 leads to

$$\Delta\mu_{QB}^b = -S_G^b(T - T_0) \tag{13}$$

By adding eqs 12 and 13, one obtains the change in chemical potential for the bulk system along the path AB

$$\Delta\mu_{AB}^b = -S_G^b(T - T_0) + RT_0 \ln\left(\frac{P^b}{P_0^b}\right) \tag{14}$$

On the other hand, in all cases, the chemical potential change for the confined system along the in-pore solid/liquid coexistence line between A(P_0^b,P_0^p,T_0) and B(P^b,P^p,T) can be decomposed as the sum of an isothermal path AQ and an isobaric path QB in the confined liquid phase. Integrating eq 5 for the confined system along the isothermal path from A(P_0^b,P_0^p,T_0) to Q(P^b,P_0^p,T_0) and the isobaric path from Q(P^b,P_0^p,T_0) to B(P^b,P^p,T) leads to

$$\begin{aligned}\Delta\mu_{AQ}^p &= \int_{P_0^p}^{P^p} V\mathrm{d}P^p \\ \Delta\mu_{QB}^p &= -\int_{T_0}^{T} S\mathrm{d}T\end{aligned} \tag{15}$$

Given that AQ is located in the confined liquid region and neglecting the pressure dependence of the confined liquid molar volume V_L^p, integration of the first equation in eq 15 leads to

$$\Delta\mu_{AQ}^p = V_L^p(P^p - P_0^p) \tag{16}$$

BQ is also located in the confined liquid region. Neglecting the temperature dependence of the entropy of the confined liquid, S_L^p, integration of the second equation in eq 15 leads to

$$\Delta\mu_{QB}^p = -S_L^p(T - T_0) \tag{17}$$

By adding eqs 16 and 17, one obtains the change in chemical potential for the confined system along the path AB

$$\Delta\mu_{AB}^p = -S_L^p(T - T_0) + V_L^p(P^p - P_0^p) \tag{18}$$

From eqs 10, 14, and 18, equating $\Delta\mu_{AB}^p = \Delta\mu_{AB}^b$ for the two situations described in Figure 7 leads, respectively, to the following coexistence conditions

$$-S_L^b(T - T_0) + RT\ln\left(\frac{P^b}{P_M^b}\right) = -S_L^p(T - T_0) + V_L^p(P^p - P_0^p) \qquad \text{(Figure 7, left)} \tag{19}$$

$$-S_G^b(T - T_0) + RT_0\ln\left(\frac{P^b}{P_0^b}\right) = -S_L^p(T - T_0) + V_L^p(P^p - P_0^p) \qquad \text{(Figure 7, right)} \tag{20}$$

which can be rewritten

$$\frac{P^b}{P_M^b} = \exp\left[(S_L^b - S_L^p)\left(\frac{T - T_0}{RT}\right)\right]\exp\left[\frac{V_L^p}{RT}(P^p - P_0^p)\right] \qquad \text{(Figure 7, left)} \tag{21}$$

$$\frac{P^b}{P_0^b} = \exp\left[(S_G^b - S_L^p)\left(\frac{T - T_0}{RT_0}\right)\right]\exp\left[\frac{V_L^p}{RT_0}(P^p - P_0^p)\right] \qquad \text{(Figure 7, right)} \tag{22}$$

These equations can be rewritten in a more convenient form as

$$P^b = K_1(T)P_M^b\exp\left[\frac{V_L^p}{RT}(P^p - P_0^p)\right] \qquad \text{(Figure 7, left)} \tag{23}$$

$$P^b = K_2(T)P_0^b\exp\left[\frac{V_L^p}{RT_0}(P^p - P_0^p)\right] \qquad \text{(Figure 7, right)} \tag{24}$$

where $K_1(T) = \exp[(S_L^b - S_L^p)((T - T_0)/RT)]$ and $K_2(T) = \exp[(S_G^b - S_L^p)((T - T_0)/RT_0)]$. Given that the entropy of the gas phase is larger than that of the liquid and that the entropy of the confined liquid is smaller than that of the bulk (due to the reduction of the number of configurations for a 2D system compared to that for a 3D system), we can write $S_G^b > S_L^b > S_L^p$. The latter inequalities combined with the fact that $T < T_0$ imply that both $K_1(T)$ and $K_2(T) < 1$ in eqs 23 and 24 (i.e., independently of whether or not the in-pore coexistence line crosses the bulk gas/liquid saturation curve). By differentiating the coexistence conditions (eqs 23 and 24) with respect to P^p at fixed temperature, we obtain

$$\mathrm{d}P^b = \frac{K_1(T)P_M^bV_L^p}{RT}\exp\left[\frac{V_L^p}{RT}(P^p - P_0^p)\right]\mathrm{d}P^p \qquad \text{(Figure 7, left)} \tag{25}$$

$$\mathrm{d}P^b = \frac{K_2(T)P_0^bV_L^p}{RT_0}\exp\left[\frac{V_L^p}{RT_0}(P^p - P_0^p)\right]\mathrm{d}P^p \qquad \text{(Figure 7, right)} \tag{26}$$

We note that $P^b < P_0^b$, so that $P^p < P_0^p$ (see Figure 7), so that the exponential terms in these equations will be less than 1. Also, $K_1(T)$ and $K_2(T)$ are both less than 1, and since V_L^p is small, $(V_L^pP^b/RT)$ will be less than 1 (except for very high bulk pressures). Thus, eqs 25 and 26 imply that a pressure change for the bulk phase corresponds to a much larger pressure change for the confined phase, $\mathrm{d}P^b \ll \mathrm{d}P^p$. This explains the strong pressure dependence of the in-pore freezing temperature; a large change in the in-pore freezing temperature with pressure can be qualitatively explained if one considers the in-pore pressure P^p instead of the bulk external pressure P^b. By making further

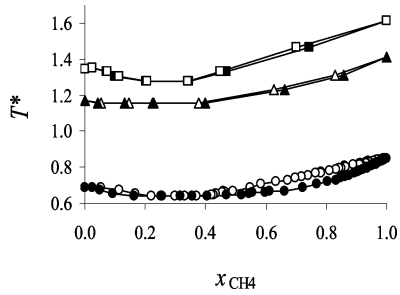

Figure 8. Solid/liquid phase diagram (T^*,x_{CH4}) for Ar/CH_4 mixtures; circles are for the bulk mixture, while triangles and squares are for mixtures confined in a slit graphite pore with $H = 2$ at $P^* = 0.002$ (~1 atm) and $P^* = 0.06$ (~25 atm), respectively. Temperatures and pressures are reduced with respect to σ_{Ar} and ε_{Ar}. Open and closed symbols denote the liquid and solid coexistence lines, respectively. The lines between the symbols are provided as a guide to the eye. The data for the bulk mixture are taken from our previous work.[34]

assumptions, Miyahara and co-workers[26] showed that the large shift in the in-pore freezing temperature with increasing pressure can be quantitatively described using the exponential relation between the bulk and in-pore pressure variations. We note that the model described above neglects effects due to strong density oscillations[46] in the confined fluid, and the tensorial nature of the pressure in the pore,[47,48] replacing the latter by an effective scalar pressure P^p. Nevertheless, the model is able to predict, qualitatively and semiquantitatively, the effect of pressure on freezing of confined fluids.

C. Freezing of the Confined Mixture. Despite a few studies of molten salts[49,50] and colloidal mixtures,[51] freezing of confined mixtures has received considerably less attention than that of pure fluids. In the present work, GCMC simulations were performed at different pressures ($P^* = 0.002$ and 0.06) to study freezing of Ar/CH_4 mixtures confined in the slit graphite nanopore with $H^* = 2$. Each simulation run consisted of simulations with parallel tempering between 16 replicas at different temperatures T^* but the same pressure P^*. In each run, the chemical potentials $\mu_{Ar}(T,P)$ and $\mu_{CH4}(T,P)$ for each replica in the parallel tempering were calculated so that the confined mixture was in equilibrium with a bulk mixture having the same molar composition, x^0_{CH4}. These conditions for the simulations correspond to the experimental process in which the confined mixture is in equilibrium with a bulk mixture having the same mole fraction. For each run, the in-pore freezing temperature was determined following the analysis reported above for pure fluids, from calculations of the orientational bond order parameter Φ_6 and the pair correlation functions $g(r)$ and $G_6(r)$. For all molar compositions studied in this work, we found that the CH_4 mole fraction for the confined mixture is always larger than that of the bulk mixture. As shown in previous works,[32,52,53] this result is due to the fact that CH_4 has a stronger interaction with the pore wall than Ar. As found for pure fluids, the average value of the 2D bond order parameter for the confined layer sharply increases at the freezing temperature (not shown). We also found that the in-pore CH_4 mole fraction, x_{CH4}, sharply increases or decreases at the freezing temperature. Such an analysis provides a first set of crystal/liquid coexistence conditions (T^*,x^L_{CH4},x^C_{CH4}).

The solid/liquid phase diagrams of Ar/CH_4 mixtures confined in the nanopore with $H^* = 2$ is shown in Figure 8 for two reduced pressures, $P^* = 0.002$ and 0.06 (~1 and 25 atm, respectively). We also report the phase diagram for the bulk mixture, which was calculated using the Gibbs−Duhem integration technique in a previous work.[34] This bulk solid/liquid phase diagram was obtained for $P^* = 0.002$, but the latter depends only weakly on pressure.[54,55] For all pressures, the phase diagram of the confined mixture is of the same type, that is, azeotropic, as that for the bulk system, but the liquid and crystal coexistence lines are located at higher temperatures. Again, the larger freezing temperature for the confined mixture compared with that of the bulk can be explained by the fact that the wall/fluid interactions are stronger than the fluid/fluid interactions for both Ar and CH_4, that is, $\alpha_{Ar} > 1$ and $\alpha_{CH4} > 1$.[12] As for pure argon and methane, it is found that the shift in the freezing temperature for the confined system depends strongly on the pressure. The model proposed in the previous paragraph remains valid in the case of mixtures and explains such a strong dependence of the in-pore freezing temperature on pressure.

TABLE 1: Azeotrope Composition x^A_{CH4} and Temperature T^A for Ar/CH_4 Mixtures Confined at $P^* = 0.002$ and 0.06 in a Slit Graphite Nanopore with $H^* = 2$ along with the Bulk Azeotrope Composition and Temperature ($H = \infty$)[a]

	$P^* = 0.002$	$P^* = 0.06$	$H = \infty$
x^A_{CH4}	0.20−0.24	0.20−0.30	0.31
T^A	1.15	1.28	0.64

[a] Due to the uncertainty in the location of the azeotrope for the confined mixture, a range of mole fractions for x^A_{CH4} is provided instead of a single value. The uncertainty for the temperature is ±0.02.

The azeotrope composition and temperature (T^A,x^A_{CH4}) for the Ar/CH_4 mixture confined at $P^* = 0.002$ and 0.06 in the nanopore with $H^* = 2$ is shown are Table 1. The location of the azeotrope has been estimated from our simulation data as follows; the crystal phase for $x_{CH4} < x^A_{CH4}$ is richer in Ar than that in the liquid phase, while the crystal phase for $x_{CH4} > x^A_{CH4}$ is richer in CH_4 than that in the liquid phase. This situation is similar to that observed for the bulk, where freezing involves an increase in x_{CH4} for mole fractions above the azeotrope composition and a decrease in x_{CH4} for mole fractions below the azeotrope composition. Due to the uncertainty in determining x^A_{CH4} from our simulation data for the confined mixtures, it was not possible to investigate accurately the dependence of the azetrope location on the pressure. Nevertheless, for all pressures, it can be seen that the azeotrope of the confined mixture is always located at a CH_4 mole fraction lower than that of the bulk mixture, $x^A_{CH4}(\infty) = 0.31$. A qualitative explanation for such a result is as follows. We know that an azeotrope appears when the coexistence line that originates from pure component 2 (having the strongest fluid/fluid interaction and therefore the highest freezing temperature; in this case, CH_4) reaches temperatures below the freezing temperature of component 1 (having the weakest fluid/fluid interaction and therefore the lowest freezing temperature; in this case, Ar). It is observed that the location of the azeotrope is shifted toward the component having the weakest fluid/fluid interaction (component 1) if the freezing temperature of component 2 is increased. Given that α is larger for methane than for argon, the increase in the freezing temperature is larger for methane than that for argon. As a result, the coexistence lines that originate from confined pure methane reach the freezing temperature of confined pure argon at a lower value of x_{CH4} than that of the bulk. Consequently, the azeotrope for the confined mixture is shifted toward the low x_{CH4} mole fractions with respect to the bulk. A deeper discussion on this issue can be found in a previous work.[34]

IV. Conclusion

In this work, we report grand canonical Monte Carlo simulations combined with the parallel tempering technique to

study the freezing of argon, methane, and their mixtures confined in a slit graphite nanopore with $H^* = 2$. The freezing temperature and structure of the confined systems are determined by calculating bond order parameters, Φ_6, and both positional $g(r)$ and bond orientational $G_6(r)$ pair correlation functions. The solid/liquid coexistence lines are located at higher temperatures than those in the bulk, as expected for these systems for which the wall/fluid interaction is stronger than the fluid/fluid interaction. In the case of the mixture, the phase diagram for the confined system is of the same type as that for the bulk (azeotrope) at all pressures. It is also found that the freezing temperatures for the confined fluids and mixture are much more strongly affected by pressure than is the case for the bulk phase. By calculating the isothermal compressibility of the confined fluid, which is found to be smaller than that of the bulk fluid, we show that such a strong effect of pressure is not expected for confined systems based on compressibility considerations. On the other hand, we show that the model originally proposed by Miyahara et al.[26] is able to describe, at least in a qualitative way, the significant shift in the in-pore freezing temperature with increasing pressure. This model, which is based on the pressure difference between the bulk and confined phases (capillary effect), is extended in the present work in order to describe any system for which an increase in the freezing temperature is observed.

Acknowledgment. We are grateful to Aziz Ghoufi for fruitful discussions. Partial support of this research was provided by U.S. National Science Foundation Grant CTS-0626031. Supercomputing time was provided by the National Partnership for Advanced Computational Infrastructure (NSF/NRAC, MCA93SO11), the National Energy Research Scientific Computing Center (DOE, DE-FGO2-98ER14847), and the High Performance Computing Center at North Carolina State University. International cooperation was supported by a NATO Collaborative Linkage Grant (No. PST. CLG.978802) and the Polish Ministry of Education and Informatics Grant N202 144 32/4235.

References and Notes

(1) For a review of effects of confinement on phase transitions, see: Gelb, L. D.; Gubbins, K. E.; Radhakrishnan, R.; Sliwinska-Bartkowiak, M. *Rep. Prog. Phys.* **1999**, *62*, 1573.

(2) Effects of confinement on freezing are reviewed in: Alba-Simionesco, C.; Coasne, B.; Dosseh, G.; Dudziak, G.; Gubbins, K. E.; Radhakrishnan, R.; Sliwinska-Bartkowiak, M. *J. Phys.: Condens. Matter* **2006**, *18*, R15.

(3) Masuda, H.; Fukuda, K. *Science* **1995**, *268*, 1466.

(4) Ajayan, P. M.; Stephan, O.; Redlich, P.; Colliex, C. *Nature* **1999**, *375*, 564.

(5) Harris, P. J. F. *Carbon Nanotubes and Related Structures. New Materials for the Twenty-First Century*; Cambridge University Press: Cambridge, U.K., 1999.

(6) Sloan, J.; Novotny, M. C.; Bailey, S. R.; Brown, G.; Xu, C.; Williams, V. C.; Fredrichs, S.; Flahaut, E.; Callender, R. L.; York, A. P. E.; Coleman, K. S.; Green, M. L. H.; Dunin-Borkowski, R. E.; Hutchison, J. L. *Chem. Phys. Lett.* **2000**, *239*, 61.

(7) Zhakidov, A. A.; Baughman, R. H.; Iqbal, Z.; Cui, C. X. *Science* **1998**, *282*, 897.

(8) Zhang, Z. B.; Gekhtman, D.; Dresselhaus, M. S.; Ying, J. Y. *Chem. Mater.* **1999**, *11*, 1659.

(9) Alcoutlabi, M.; McKenna, G. B. *J. Phys.: Condens. Matter* **2005**, *17*, R461.

(10) Eyraud, C.; Quinson, J. F.; Brun, M. *Characterization of Porous Solids*; Unger, K., Rouquerol, J., Sing, K. S. W., Kral, H., Eds.; Elsevier: Amsterdam, The Netherlands, 1988; p 307.

(11) Radhakrishnan, R.; Gubbins, K. E.; Sliwinska-Bartkowiak, M. *J. Chem. Phys.* **2000**, *112*, 11048.

(12) Radhakrishnan, R.; Gubbins, K. E.; Sliwinska-Bartkowiak, M. *J. Chem. Phys.* **2002**, *116*, 1147.

(13) Warnock, J.; Awschalom, D. D.; Shafer, M. W. *Phys. Rev. Lett.* **1986**, *57*, 1753.

(14) Evans, R.; Marini Bettolo Marconi, U. *J. Chem. Phys.* **1987**, *86*, 7138.

(15) Sliwinska-Bartkowiak, M.; Gras, J.; Sikorski, R.; Radhakrishnan, R.; Gelb, L. D.; Gubbins, K. E. *Langmuir* **1999**, *15*, 6060.

(16) Radhakrishnan, R.; Gubbins, K. E.; Watanabe, A.; Kaneko, K. *J. Chem. Phys.* **1999**, *111*, 9058.

(17) Klein, J.; Kumacheva, E. *Science* **1995**, *269*, 816.

(18) Kumacheva, E.; Klein, J. *J. Chem. Phys.* **1998**, *108*, 7010.

(19) Watanabe, A.; Kaneko, K. *Chem. Phys. Lett.* **1999**, *305*, 71.

(20) Kaneko, K.; Watanabe, A.; Iiyama, T.; Radhakrishnan, R.; Gubbins, K. E. *J. Phys. Chem. B* **1999**, *103*, 7061.

(21) Miyahara, M.; Gubbins, K. E. *J. Chem. Phys.* **1997**, *106*, 2865.

(22) Maddox, M.; Gubbins, K. E. *J. Chem. Phys.* **1997**, *107*, 9659.

(23) Raviv, U.; Laurat, P.; Klein, J. *Nature* **2001**, *413*, 51.

(24) Raviv, U.; Giasson, S.; Frey, J.; Klein, J. *J. Phys.: Condens. Matter* **2002**, *14*, 9275.

(25) Mugele, F.; Persson, B.; Zilberman, S.; Nitzan, A.; Salmeron, M. *Tribol. Lett.* **2002**, *12*, 123.

(26) Miyahara, M.; Kanda, H.; Shibao, M.; Higashitani, K. *J. Chem. Phys.* **2000**, *112*, 9909.

(27) Kanda, H.; Miyahara, M.; Higashitani, K. *J. Chem. Phys.* **2004**, *120*, 6173.

(28) Kanda, H.; Miyahara, M.; Higashitani, K. *Adsorption* **2005**, *11*, 295.

(29) Koga, K.; Gao, G. T.; Tanaka, H.; Zeng, X. C. *Nature* **2001**, *412*, 802.

(30) Takaiwa, D.; Hatano, I.; Koga, K.; Tanaka, H. *Proc. Natl. Acad. Sci. U.S.A.* **2008**, *105*, 39.

(31) Frenkel, D.; Smit, B. *Understanding Molecular Simulation*, 2nd ed.; Academic: New York, 2002.

(32) Coasne, B.; Czwartos, J.; Gubbins, K. E.; Hung, F. R.; Sliwinska-Bartkowiak, M. *Mol. Phys.* **2004**, *19*−*20*, 2149.

(33) Coasne, B.; Czwartos, J.; Gubbins, K. E.; Hung, F. R.; Sliwinska-Bartkowiak, M. *Adsorption* **2005**, *11*, 301.

(34) Czwartos, J.; Coasne, B.; Gubbins, K. E.; Hung, F. R.; Sliwinska-Bartkowiak, M. *Mol. Phys.* **2005**, *21*−*23*, 3103.

(35) Steele, W. A. *Surf. Sci.* **1973**, *36*, 317.

(36) Johnson, J. K.; Zollweg, J. A.; Gubbins, K. E. *Mol. Phys.* **1993**, *78*, 591.

(37) Hung, F. R.; Coasne, B.; Santiso, E. E.; Gubbins, K. E.; Siperstein, F. R.; Sliwinska-Bartkowiak, M. *J. Chem. Phys.* **2005**, *122*, 144706.

(38) Radhakrishnan, R.; Gubbins, K. E. *Mol. Phys.* **1999**, *96*, 1249.

(39) Hung, F. R.; Dudziak, F. R.; Sliwinska-Bartkowiak, M.; Gubbins, K. E. *Mol. Phys.* **2004**, *102*, 223.

(40) (a) Halperin, B. I.; Nelson, D. R. *Phys. Rev. Lett.* **1978**, *41*, 121. (b) Nelson, D. R.; Halperin, B. I. *Phys. Rev. B* **1979**, *19*, 2457. (c) Young, A. P. *Phys. Rev. B* **1979**, *19*, 1855.

(41) Strandburg, K. J. *Rev. Mod. Phys.* **1988**, *60*, 161.

(42) Yan, Q.; de Pablo, J. J. *J. Chem. Phys.* **1999**, *111*, 9509.

(43) Kofke, D. A. *J. Chem. Phys.* **1993**, *98*, 4149.

(44) Agrawal, R.; Kofke, D. A. *Mol. Phys.* **1995**, *85*, 43.

(45) Allen, M. P.; Tildesley, D. J. *Computer Simulation of Liquids*; Clarendon: Owford, U.K., 1987; p 54.

(46) Evans, R. *J. Phys.: Condens. Matter* **1990**, *2*, 8989.

(47) Dominguez, H.; Allen, M. P.; Evans, R. *Mol. Phys.* **1999**, *96*, 209.

(48) Koga, K. *J. Chem. Phys.* **2002**, *116*, 10882.

(49) Meyer, R. R.; Sloan, J.; Dunin-Borkowski, R. E.; Kirkland, A. I.; Novotny, M. C.; Bailey, S. R; Hutchinson, J. L.; Greene, M. L. H. *Science* **2000**, *289*, 1324.

(50) Wilson, M. *J. Chem. Phys.* **2002**, *116*, 3027.

(51) Cui, S. T.; McCabe, C.; Cummings, P. T.; Cochran, H. D. *J. Chem. Phys.* **2003**, *118*, 8941.

(52) Tan, Z.; Gubbins, K. E. *J. Chem. Phys.* **1992**, *96*, 845.

(53) Cracknell, R. F.; Nicholson, D. A.; Quirke, N. *Mol. Phys.* **1993**, *80*, 885.

(54) Lamm, M. H.; Hall, C. K. *Fluid Phase Equilib.* **2001**, *182*, 37.

(55) Lamm, M. H.; Hall, C. K. *Fluid Phase Equilib.* **2002**, *194*−*197*, 197.

JP9031699